**REVIEW**

# Functional-Material-Based Touch Interfaces for Multidimensional Sensing for Interactive Displays: A Review

**Shuo Gao**<sup>1,2\*</sup>

1. Hetero-Genesys Laboratory, Department of Engineering, University of Cambridge, Cambridge CB3 0FA, U.K
2. School of Instrumentation and Optoelectronic Engineering, Beihang University, Beijing, 100083, China

## ARTICLE INFO

*Article history*

Received: 5 September 2019

Accepted: 12 October 2019

Published Online: 30 October 2019

*Keywords:*

Touch interfaces

Functional materials

Multidimensional sensing

Interactive displays

## ABSTRACT

Multidimensional sensing is a highly desired attribute for allowing human-machine interfaces (HMIs) to perceive various types of information from both users and the environment, thus enabling the advancement of various smart electronics/applications, e.g., smartphones and smart cities. Conventional multidimensional sensing is achieved through the integration of multiple discrete sensors, which introduces issues such as high energy consumption and high circuit complexity. These disadvantages have motivated the widespread use of functional materials for detecting various stimuli at low cost with low power requirements. This work presents an overview of simply structured touch interfaces for multidimensional (x-y location, force and temperature) sensing enabled by piezoelectric, piezoresistive, triboelectric, pyroelectric and thermoelectric materials. For each technology, the mechanism of operation, state-of-the-art designs, merits, and drawbacks are investigated. At the end of the article, the author discusses the challenges limiting the successful applications of functional materials in commercial touch interfaces and corresponding development trends.

**1. Introduction**

**T**OUCH panels have become must-have components in interactive displays, which come equipped in most current consumer electronics, e.g., smartphones<sup>[1-20]</sup>. Traditional touch panels detect a user's touch locations in 2 dimensions (on the x and y axes) by employing various techniques, such as resistive, capacitive, and optical-related architectures, resulting in highly effective human-machine interactions. However, developments in electronics and information technology are requiring much larger volumes of data to be acquired from and input into end terminals, resulting in user dis-

satisfaction with conventional 2-dimensional sensing. Hence, there is a need for multidimensional sensing. Additional components are usually integrated into interactive displays to achieve this goal. For example, a capacitive force sensor is included underneath the original capacitive touch panel for 3-dimensional (x-y-z) sensing in the iPhone 6S<sup>[21]</sup>. However, the integration of multiple sensors for multidimensional sensing gives rise to many issues, such as increased product volume, complex circuitry, and higher power consumption. Among these issues, power consumption is already a concern for interactive displays and leads to short battery lifetimes.

\*Corresponding Author:

Shuo Gao,

Hetero-Genesys Laboratory, Department of Engineering, University of Cambridge, Cambridge CB3 0FA, U.K; School of Instrumentation and Optoelectronic Engineering, Beihang University, Beijing, 100083, China;

Email: [shuo\\_gao@buaa.edu.cn](mailto:shuo_gao@buaa.edu.cn)

To avoid the issues raised by the integration of multiple sensors, functional materials are starting to be used to assemble simply structured multifunctional touch panels for multidimensional sensing. For example, researchers at the University of Cambridge have presented a multifunctional touch panel constructed from flexible graphene/polyvinylidene fluoride (PVDF)/graphene sandwiched layers that is capable of simultaneously detecting capacitive and force touch signals. This extremely simple structure enables the user to input 3-dimensional information without incurring any additional power consumption or circuit complexity<sup>[22]</sup>. Many other functional-material-based touch panels for multidimensional sensing have also been reported in the literature<sup>[22-34]</sup>. Due to their desirable attributes, such as simple structures, low power requirements and low cost, functional-material-based touch interfaces have a strong potential for widespread use not only in interactive displays but also on a larger stage, e.g., in smart cities<sup>[35]</sup>. To provide readers with a picture of how functional materials can help touch panels detect a variety of external stimuli, in this article, we summarize the state-of-the-art multifunctional touch interfaces and then discuss the challenges limiting their successful use in commercial products.

This paper is structured as follows. Section II presents a review of functional-material-based touch panels for force and temperature sensing. The reviewed techniques are compared in Section III. Section IV discusses the limitations of applying functional materials for multidimensional sensing, based on which possible development trends for multifunctional touch panels are proposed.

## 2. Functional-Material-Based Multifunctional Touch Panels for Multidimensional Sensing

### 2.1 Force Sensing

Force sensing is a function that has recently been incorporated into touch panels for interactive displays. This function was successfully commercialized in 2015 with the iPhone 6S<sup>[21]</sup> by employing a capacitive technique<sup>[21]</sup>. However, three major issues prevented it from satisfying the increasing needs of users. First, the detection sensitivity and resolution of the system are low; only two force levels can be recognized. Second, the detection of multiple force touches is not supported. Third, the force levels cannot be interpreted immediately, limiting its use in complex software environments, e.g., real-time games. To address the above issues, piezoelectric, piezoresistive and triboelectric techniques have been presented in the literature. These techniques will be reviewed in this section.

### 2.1.1 Piezoelectric Force Sensing

Piezoelectricity is the phenomenon by which a charge is generated in certain solid materials when mechanical stress is applied<sup>[22,24]</sup>. It was first demonstrated in 1880 by C. Linnaeus and F. Aepinus. The working principle of piezoelectric materials is based on their noncentrosymmetric structures<sup>[22]</sup>. When a load force is applied to a centrosymmetric material, its polarization remains intact. In contrast, the polarization of a noncentrosymmetric material becomes either positive or negative depending on the direction of the applied force, inducing a charge in the material. This is illustrated in Figure 1 a. The structure of PVDF in the  $\beta$  phase is shown in Figure 1 b as an example.

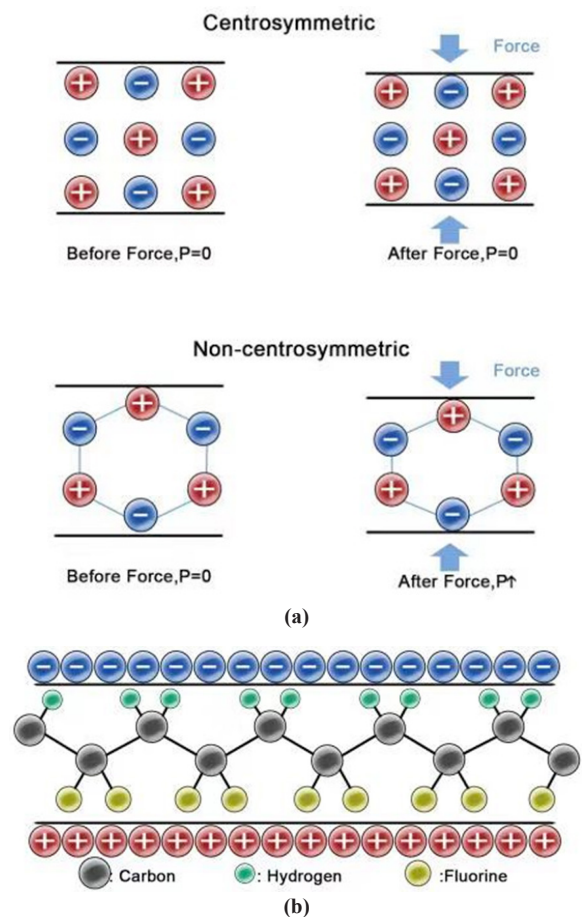


**Figure 1.** (a) Working principle of the noncentrosymmetric induced piezoelectric effect. (b) Structure of  $\beta$ -phase PVDF

Conventional piezoelectric materials include PVDF<sup>[36-38]</sup> and its copolymers, zinc oxide (ZnO)<sup>[39-40]</sup>, barium titanate (BaTiO<sub>3</sub>)<sup>[41-42]</sup>, and lead zirconate titanate (PZT)<sup>[43-44]</sup>. Their piezoelectric coefficients are listed in Table 1. To enhance the piezoelectric coefficient of PVDF, this material can be modified by introducing other monomers on

the polymer chain; for example, trifluoroethylene (TrFE) can be introduced, creating the P(VDF-TrFE) copolymer, as listed in Table 1. The bulky TrFE loosens the structure of the copolymer, causing the dipoles to be more easily reoriented under an external applied force [45]. Such materials are widely used for force sensing in a vast number of applications, ranging from industrial electronics [46,47] to commercial electronics [48,49]. The relationship between the applied force and the induced charge can be expressed as follows [22]:

$$Q = \frac{d_{33}F}{A} \tag{1}$$

where Q is the force-induced charge,  $d_{33}$  is the piezoelectric coefficient in the z direction, F is the applied force and A is the contact area. The force amplitude can be interpreted by integrating Q. Piezoelectric-material-based force touch panels have been widely reported in the literature [22,23,25,27]. Some of the most widely used piezoelectric materials in interactive displays are PVDF and its copolymer P(VDF-TrFE) because of their high piezoelectric coefficients, good mechanical properties and optical transparency [22] (note that as listed in Table 1, PZT and BaTiO<sub>3</sub> have much higher dielectric constants, but ceramics are brittle, especially when fabricated as large-area panels with small thicknesses; hence, they are not widely used for force touch panels).

**Table 1.** Typical Piezoelectric Materials and Their  $d_{33}$  Values

Material	$d_{33}$ (nC/N)
PVDF	24-34
P(VDF-TrFE)	25-40
ZnO	12-13
PZT	225-590
BaTiO <sub>3</sub>	191

To accurately interpret the applied force, an accurate  $d_{33}$  value is necessary. Hence, techniques for precisely measuring  $d_{33}$  have been developed for different types of piezoelectric materials, namely, films and ceramics. In general, for the former, four techniques are widely used: the Berlincourt method for the direct measurement of stress-induced electric signals [49], laser interferometers [49] and laser scanning vibrometers [49] for the measurement of changing electric-field-induced displacements, and piezoelectric force microscopes [51] for the imaging and manipulation of piezoelectric/ferroelectric material domains. Among them, the Berlincourt method is still controversial with regard to its suitability for characterizing the piezoelectric coefficients of thin films because of the challenge of avoiding bending effects when applying a homoge-

neous uniaxial stress to a thin film clamped on a thick substrate. To eliminate such undesired bending effects, various modifications (e.g., a pneumatic pressure rig [50]) have been applied to the original Berlincourt method. For ceramics, the most widely adopted technique for probing the piezoelectric coefficient is the Berlincourt method.

Two architectures are widely used. In the first, the piezoelectric layer lies underneath a conventional capacitive layer, endowing a conventional capacitive touch panel with a force sensing function [52]. A typical structure is shown in Figure 2 a; this structure was proposed in [54] and has been applied in commercial products (Figure 2 b [54]). In the second architecture, the piezoelectric layer replaces the insulating layer of a capacitive touch panel, transforming the capacitive touch panel into a piezoelectric force touch panel [23,24,55,56]. The former architecture has the advantage of a high detection resolution in 2 dimensions since the capacitive sensing function is not affected. The latter avoids increasing the touch panel's thickness but loses detection accuracy on the x and y axes – many studies have reported designs with high force touch sensitivities and resolutions but have failed to evaluate their performances in 2D detection [23,55]. Nevertheless, a recent study in Cambridge has demonstrated the ability to maintain the capacitive sensing function by employing different sensing frequencies (as shown in Figure 2 c and d) for capacitive and force sensing when using the second architecture.

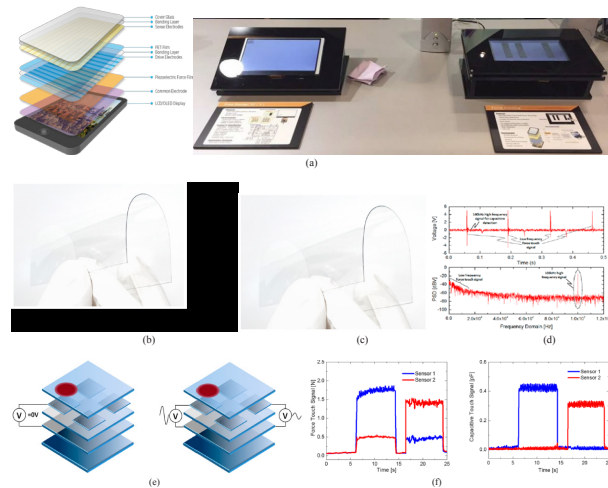


**Figure 2.** (a) Piezoelectric touch panel proposed in [53] and the corresponding product shown at CES 2017. (b) Sandwich structure of the PVDF-based touch panel proposed in [22] and (c) the fabricated flexible touch panel. (d) Time- and frequency-domain properties of the capacitive signal [22] and the piezoelectric force touch signal [22]. (e) Challenges related to static force touches and force-touch-induced stress propagation [22]. (f) Elimination of false force touches by employing the capacitive signal [22].

Piezoelectric materials face two major challenges when used for force sensing in interactive displays: a static force touch cannot be read, and force-induced stress propagation may give rise to false force touch signals (as conceptually illustrated in Figure 2 e) [22,56]. To address these challenges, comprehensive algorithms have been developed that exploit the capacitive touch signal [22]. This is one of the advantages of multidimensional sensing: because changes are detected in multiple physical parameters, it may be possible to compensate for the drawbacks of one desired signal (the force signal, in this case) by finding its correlations with signals in other dimensions (the capacitive signal, in this case).

### 2.1.2 Piezoresistive Force Sensing

The piezoresistive technique is an alternative solution for force sensing. The resistivity (R) of a piezoresistive material is altered when the material suffers mechanical strain [57]. The strain sensitivity is typically described by a gauge factor (GF) [57]:

$$GF = \Delta R / R_0 / \varepsilon \tag{2}$$

where  $\Delta R$  denotes the change in resistance,  $R_0$  is the unstrained resistance, and  $\varepsilon$  is the strain.

The piezoresistive technique is capable of both dynamic and static force sensing [57-63]. However, the piezoresistive technique is an active sensing technique, with considerable energy consumption during operation, and the thermal noise arising from the resistance of the piezoresistive material degrades its detection sensitivity. The accumulated heat generated during detection is also undesirable for interactive displays.

Unlike piezoelectric materials, which exhibit dielectric properties, piezoresistive materials can directly work as electrodes due to their relatively low sheet resistance (e.g.,  $2 \text{ K}\Omega/\square$  [61]). Two types of widely used piezoresistive electrodes are PEDOT:PSS [62] and fabrics [61]. Between them, PEDOT:PSS is more suitable for display applications due to its good optical transparency [63]. As illustrated in Figure 3 a and b [62], for touch interface applications, PEDOT:PSS can be patterned into zigzag-shaped electrodes, simplifying the touch panel structure and reducing the stacking thickness. The change in the resistivity is proportional to the applied strain, as shown in Figure 3 c. However, the 2-dimensional x-y sensing resolution of this system is strongly constrained because the panel supports only nine piezoresistive electrode touch locations. To achieve a high 2D detection resolution, the authors of [28] assembled a touch panel system in which a look-up table was used to assist four piezoresistive sensors (Figure 3 f) in interpret-

ing the force amplitudes and touch locations. This system achieved a high 2D spatial resolution of 2 mm and a force detection sensitivity of 10 mN, as shown in Figure 3 e, allowing user needs to be satisfied by a finger touch. Furthermore, the experimental results also demonstrated high stability of the force touch responsivity, as seen by examining the electrical outputs generated by two touch objects with different contact areas (as shown in Figure 4 g).

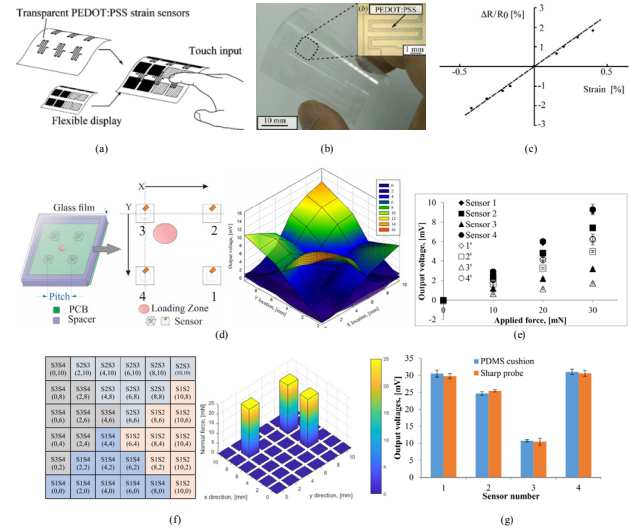


**Figure 3.** PEDOT:PSS based force touch panel – (a) the conceptual structural description and (b) a photograph of a real sample based on (a) [50]. (b) Experimental results for the strain-resistance responsivity [50]. (d) Schematic description of the basic sensor array proposed in [28] and test results from the sensor array. (e) Test results obtained with and without the cover film [28]. (f) Plots of force and location information for the sensor array proposed in [28]. (g) Force-voltage responsivities for two different touch objects [28].

### 2.1.3 Triboelectric Force Sensing

The triboelectric effect has been observed for several thousand years; however, its working principle is still under investigation. A broadly accepted explanation is that chemical bonds are created between two surfaces of two different materials when they come in contact [64]. Hence, charges (electrons, ions or molecules) are transferred to balance the electrochemical potentials of the surfaces. When the materials are separated, a portion of the bonded atoms prefer to hold extra electrons, while some of their counterparts are willing to give electrons away, possibly giving rise to triboelectric charges on the materials' surfaces. The sign of the total charge concentrated on the surface of one material is determined by the material's polarity relative to the other. A strong triboelectric effect normally occurs with insulators and less conductive materials

<sup>[64]</sup>. Therefore, charge can be accumulated and maintained on the material surfaces for a considerable time, resulting in the formation of electrostatic charges. Traditionally, the triboelectric effect is deemed undesirable, and it can cause damage in a broad range of areas, such as electronics, human life, and industrial processes <sup>[65-67]</sup>. Nevertheless, recently developed techniques have smartly utilized the triboelectric effect as a green energy source for energy harvesting <sup>[68-72]</sup> and touch sensing <sup>[74-79]</sup>.

As introduced above, the triboelectric effect is a contact-based phenomenon; hence, in general, there are two main modes of generating triboelectric charges: the contact-separation mode and the lateral-sliding mode (two other modes – the rotation mode and the single-electrode mode – can be regarded as special cases of the contact-separation mode and lateral-sliding mode and hence are not introduced here) <sup>[64]</sup>. In each mode, two cases can be considered: the dielectric-to-dielectric case and the metal-to-dielectric case. Below, only the mechanism of the vertical contact-separation mode is briefly explained, as this mode is widely used in touch panels.

#### (1) Dielectric-to-Dielectric Case

The coupled effects of contact charging and electrostatic induction are employed to explain the working principle in the dielectric-to-dielectric case. In Figure 4 a, the operational process in the dielectric-to-dielectric case is conceptually depicted. Here,  $M_1$  and  $M_2$  indicate two materials in different triboelectric series. The thicknesses of the two materials are  $d_1$  and  $d_2$ , respectively. The separation distance is  $d_3$ . In the initial state, the electric potential difference (EPD) is 0. When the surfaces come in contact due to an external applied force, charges with different signs are generated due to surface charge transfer. The EPD remains 0 in the contact state ( $d_3 = 0$ ) and starts to become either positive or negative during the releasing action, depending on the positions of  $M_1$  and  $M_2$  in the triboelectric series. For ease of description,  $M_1$  is assumed to be Kapton, and  $M_2$  is assumed to be poly(methyl methacrylate) (PMMA) <sup>[64]</sup>; hence, net positive and negative charges arise at the PMMA surface and the Kapton surface, respectively. The EPD reaches its maximum value once the two materials have been completely released, drops when the materials are approaching each other again due to the external force, and eventually returns to 0 when the two materials are in contact. Under the assumption that the bottom electrode is grounded, the electric potential read from the top electrode is <sup>[64]</sup>

$$V_{\text{Top}} = -\frac{\sigma \Delta d}{\epsilon_0} \quad (3)$$

where  $\sigma$  is the triboelectric charge density,  $\Delta d$  is the distance between  $M_1$  and  $M_2$  in a given state, and  $\epsilon_0$  is the permittivity of vacuum.

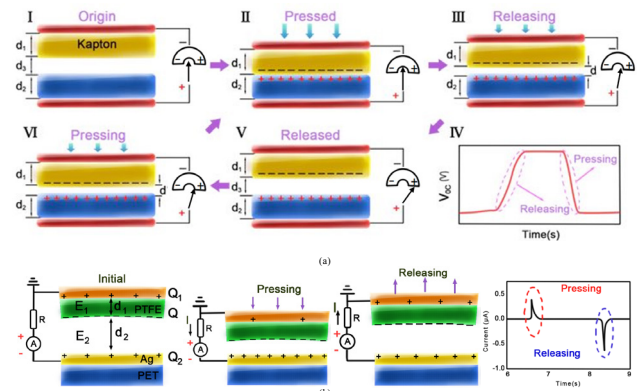


**Figure 4.** Working principle of the contact-separation mode of triboelectric charge generation: (a) the dielectric-to-dielectric case and (b) the metal-to-dielectric case <sup>[64]</sup>

#### (2) Metal-to-Dielectric Case

With regard to the metal-to-dielectric architecture, a representative case <sup>[80]</sup> is illustrated in Figure 4 b, in which an external resistor  $R$  is used to construct the equivalent circuit. Based on the triboelectric series, a net negative charge forms on the polytetrafluoroethylene (PTFE) surface. Here,  $\sigma$ ,  $\sigma_1$  and  $\sigma_2$  represent the charge densities of the PTFE, Cu and Ag surfaces, respectively;  $d_1$  and  $d_2$  are the thickness of the PTFE layer and the separation distance, respectively; and the relationships among these quantities are described as follows <sup>[80]</sup>.

$$\sigma_1 = -\frac{\sigma}{1 + \frac{d_1}{d_2 \epsilon_{\text{TP}}}} \quad (4)$$

$$\sigma_2 = -\sigma - \sigma_1 \quad (5)$$

$\epsilon_{\text{TP}}$  is the permittivity of the PTFE. Because the charge  $Q$  is constrained to the surface of the PTFE, the charge density at the Cu layer depends on the distance  $d_2$ . Therefore, when the surfaces are pressed together at a certain force level, an instantaneous current is generated, and the current value can be employed to interpret the force level.

Studies on triboelectrification report that under the same external force touch and for the same touch panel architecture, the amplitude of the triboelectric signal is positively correlated with the triboelectric series <sup>[32]</sup>, the surface roughness <sup>[74]</sup>, and the contact area <sup>[32]</sup>. The first influence is related to the nature of the chosen materials, as shown in Figure 5 a, which remains constant after being selected. Hence, to boost the mechanical-to-electrical conversion efficiency, the contact surface is usually

patterned to increase its roughness, and the contact area is suitably designed to have the desired power generation performance. For example, in the design shown in Figure 5 b, the PDMS layer is patterned with micropyramids to enhance its surface roughness<sup>[75]</sup>. Figure 5 c demonstrates the transparency and flexibility of this structure and its use in a smartphone. The effect of the contact area was studied in<sup>[32]</sup> by fabricating a single-electrode triboelectric touch panel composed of a PDMS panel surface and 36×20 gold electrodes, as shown in Figure 5 e. The relationship between electrode size and triboelectricity was experimentally studied (Figure 5 d). It was observed that for a given touch object, as the electrode size increases, the triboelectric signal is proportionally enhanced, in agreement with theoretical findings<sup>[76]</sup>. A “6”-shaped object was successfully recognized by the fabricated touch panel (Figure 5 f). However, the 2-dimensional resolution is reduced, and cross-talk may become a major issue as the electrode area is gradually increased. Hence, comprehensive consideration of the electrode design is required during product design for specific purposes.

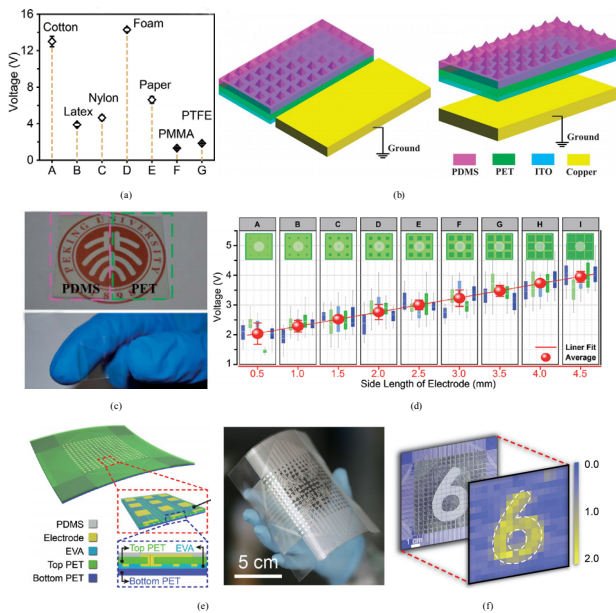


**Figure 5.** (a) Triboelectric induced electric signals based on different contact materials<sup>[75]</sup>. (b) Structure of a triboelectric touch panel and its patterned surface for increased surface roughness<sup>[75]</sup>. (c) Fabricated triboelectric touch interface with the structure shown in (b). (d) Experimental results for the voltage boost due to increasing contact area<sup>[32]</sup>, where A – I represent the different touch areas. (e) Structure of a single-electrode-based triboelectric touch panel and a photograph of the real prototype<sup>[32]</sup>. (f) The electrical signal induced by a “6”-shaped object on the triboelectric touch interface presented in (e)<sup>[32]</sup>

## 2.2 Temperature Sensing

Temperature sensing can be achieved by pyroelectric and thermoelectric means, which enable the passive detection of the temperature difference between a human finger and a touch panel<sup>[81-83]</sup>. The absolute finger temperature has not yet been obtained in the literature. Instead, the x-y locations are detected by determining the locations of thermal shifts. Although only 2-dimensional sensing has been achieved in current work, these two techniques are still treated as an additional dimension of sensing since they truly detect a different physical stimulus, and it will be possible to interpret the absolute temperature value of a touch once the surface temperature of the panel can be estimated.

### 2.2.1 Pyroelectric Temperature Sensing

Pyroelectricity refers to the generation of a temporary voltage in certain noncentrosymmetric materials when a temperature difference occurs<sup>[84-88]</sup>. The change in temperature alters the polarization of the material, giving rise to a voltage across the material (e.g., a crystal). The direction of the voltage is determined by the sign of  $\Delta T$ <sup>[87]</sup>. Among the 32 possible point group symmetries, 10 of them offer pyroelectric properties, namely, the triclinic (1), monoclinic (2, m), orthorhombic (2mm), tetragonal (4, 4mm), trigonal (3, 3m), and hexagonal (6, 6mm) symmetries. Widely used pyroelectric materials include ZnO, PVDF and its copolymers, triglycine sulfate (TGS), and lithium tantalite ( $\text{LiTaO}_3$ )<sup>[87]</sup>.

In scalar form, the change in polarization  $\Delta P_s$  caused by the pyroelectric effect can be calculated from the pyroelectric coefficient  $p$  and the temperature shift  $\Delta T$  as follows<sup>[87]</sup>:

$$\Delta P_s = p \Delta T \quad (6)$$

As briefly mentioned previously, a change in temperature generates an electric field through the pyroelectric effect. The  $\Delta T$ -induced charge can be measured as a current, which is described as<sup>[87]</sup>

$$i = A p dT / dt \quad (7)$$

where  $A$  is the surface area of the device and  $dT/dt$  is the rate of the change in temperature with respect to time. Hence, only dynamic temperature changes can be detected. Conventional measurement techniques include rapid laser modulation heating (the Chynoweth method) and the slow heating/cooling method. In the former, a 5 mW He-Ne laser is used to heat the sample, and the generated current is detected by a lock-in amplifier<sup>[87]</sup>. In the

latter method, a temperature-stabilized chamber is used to provide a constant heating or cooling rate, normally from 0.5 to 4 °C/min. The pyroelectric current is collected and amplified by a current amplifier<sup>[87]</sup>. The energy required to dynamically alter the temperature can originate from either electromagnetic radiation or the heat induced by the reaction of chemical species, based on which a variety of low-power and low-cost applications have been developed, such as intruder/fire alarms, gas analysis instruments, radiometers and laser detectors<sup>[89-95]</sup>.

It is worth mentioning that all pyroelectric materials also exhibit piezoelectric properties. In these materials, the piezoelectric effect and the pyroelectric effect are strongly correlated because they are both related to polarization. Taking PVDF as an example, the piezoelectric coefficient  $d_{33}$  and the pyroelectric coefficient  $p_3$  are expressed as<sup>[86]</sup>

$$d_{33} = 2\varepsilon_{33}\varepsilon_0k_{33}P_s \quad (8)$$

$$p_3 = -\varepsilon_{33}\beta P_s \quad (9)$$

where  $k_{33}$  is the quadratic electrostriction coefficient and  $\beta$  is the inverse Curie constant. The above equations explain why the piezoelectric coefficient has approximately the same frequency response as the dielectric constant does and why the hysteresis loops of  $d_{33}$  and the pyroelectric current overlap<sup>[87]</sup>.

As explained above, although the working principles of the piezoelectric and pyroelectric effects are different, they do share some similarities, such as the following:

(1) The piezoelectric and pyroelectric coefficients are both constants associated with the environmental temperature and frequency<sup>[86-87]</sup>.

(2) The clamping of a thin film such as PVDF results in a decrease in both the pyroelectric and piezoelectric coefficients to a small fraction of their values in the unclamped state.

(3) A secondary effect becomes significant when a ferroelectric device is subjected to an AC radiation flux at one of the device's resonant frequencies, giving rise to an enormous boost in the piezoelectric and pyroelectric coefficients.

Additionally, due to the coexistence of the piezoelectric and pyroelectric effects in ferroelectric materials, several drawbacks arise when ferroelectric devices are used for single-dimensional sensing, e.g., force sensing. This situation will be discussed in detail in the last section.

In<sup>[23]</sup>, sandwich-structured touch panels were assembled using PVDF as a temperature sensing layer and various flexible conductive materials as electrodes (graphene screen/inkjet ink (thick and thin) and carbon nanotubes

(CNTs)/xylan ink), as shown in Figure 6 b. The pyroelectric response of sample S5 is illustrated in Figure 6 c, where the positive and negative curves demonstrate its temperature sensing capabilities.

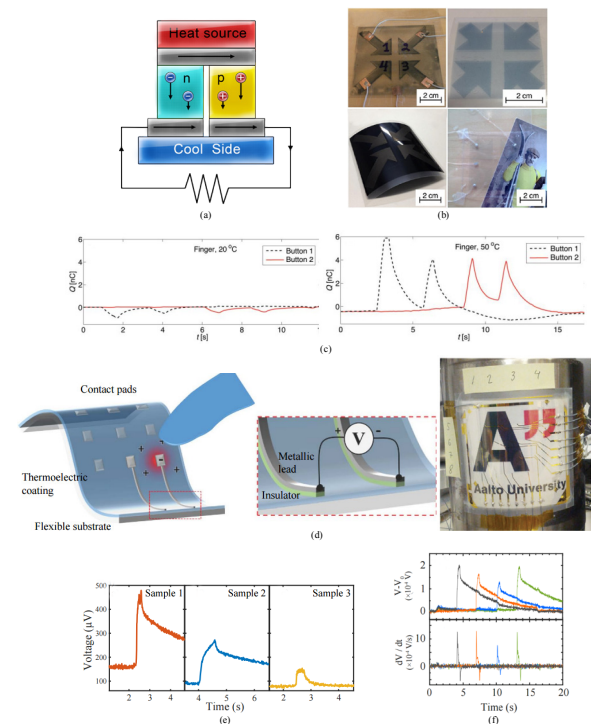


**Figure 6.** (a) Working principle of the Seebeck effect. (b)

Sandwich-structured touch panels with different electrode materials reported in<sup>[23]</sup>. (c) Finger-touch-induced pyroelectric signals. (d) Structure and photograph of the thermoelectric touch panel presented in<sup>[29]</sup>. (e) Touch-generated voltages for different samples in<sup>[29]</sup>. (f) Successful cross-talk elimination with a thermoelectric technique<sup>[29]</sup>.

The pyroelectric response signal is proportional to the temperature difference between the finger/stylus and the touch panel, whereas the piezoelectric response is proportional to the applied force. Typically, the pyroelectric effect occurs at lower frequencies than the piezoelectric effect due to the slow heat transfer mechanism<sup>[23]</sup>.

## 2.2.2 Thermoelectric Temperature Sensing

Thermoelectric materials have become a focus of research in the last twenty years due to their intrinsic ability to convert conventional wasted heat into electricity<sup>[96-100]</sup> through the Seebeck effect, providing a potential solution for sustainable energy. The working principle of the Seebeck effect is that when heat is applied to one side of a conductive or semiconductive material, electrons have a tendency to flow to the relatively cold side. When two different conductive or semiconductive materials are connected to form a loop, an electric current is present

because of the distinct changes in the electron energy levels in each material; therefore, an EPD is created at each junction. To enhance this effect, n-type and p-type semiconductors are widely used to form a structure such as that shown in Figure 6 a. The thermoelectric performance is quantified by a dimensionless figure of merit:

$$zT = \alpha^2 \sigma T / (\kappa_e + \kappa_L) \tag{10}$$

where  $\alpha$  is the Seebeck coefficient,  $\sigma$  is the electrical conductivity,  $T$  is the absolute temperature, and  $\kappa_e$  and  $\kappa_L$  are the electronic and lattice contributions, respectively, to the total thermal conductivity  $\kappa$  [100]. Widely used families of thermoelectric materials include tetradymites, alloys with the general composition  $(\text{Bi,Sb})_2(\text{Te,Se})_3$ , and lead salts. Some representative materials are summarized in [100], along with their corresponding  $zT$  values and working temperature ranges.

A variety of applications of the thermoelectric effect have been developed and put into practical use, such as energy generators, coolers and temperature sensors [100-105].

In [29], a thermoelectric touch panel for location detection was presented based on the temperature difference between the touched pad and an adjacent pad. This temperature difference generates a potential difference between the pad wires, as conceptually shown in Figure 6 d. ZnO thin films were deposited on three different substrates – PET, glass and Kapton (named sample 1, sample 2 and sample 3, respectively) – resulting in Seebeck coefficients of -73, -119, and -44  $\mu\text{V/K}$ , respectively. The experimental results for glove touches, as illustrated in Figure 6 e, demonstrated the successful interpretation of the touch signals. Cross-talk between adjacent electrodes was also studied in [29], and promising results were obtained, as shown in Figure 6 f, indicating that good elimination can be achieved with thermoelectric techniques.

### 3. Comparison and Potential Applications

In the above paragraphs, touch panels based on piezoelectric, piezoresistive, triboelectric, pyroelectric and thermoelectric materials for multidimensional sensing have been reviewed. Before proceeding to the next section, which discusses the challenges related to the practical use of such devices and corresponding development trends, these technologies are first compared here from the perspectives of functionality, N-dimensional sensing, power consumption and performance stability under extreme conditions, and potential application scenarios are then presented.

As previously explained, these technologies can be divided into two main categories: force sensing and temperature sensing. Force sensing is broadly recognized as

a type of 3-dimensional sensing, as compared to conventional 2-dimensional position sensing [21-22,25]. However, pyroelectric- and thermoelectric-based temperature sensing are still treated as 2-dimensional sensing methods since these two technologies are utilized not for determining an absolute temperature value but for detecting the temperature difference between the touch object and the touch panel to detect the touch location.

With regard to power consumption, most of these technologies detect touch-induced signals passively, with the exception of piezoresistive force sensing, which requires a stable power supply (e.g., a battery), resulting in higher power consumption compared to its counterparts. The multitouch capability has become important in interactive interfaces and has been supported in capacitive touch panels for the last decade. For the technologies discussed in this article, multitouch is always supported. However, for the piezoelectric, pyroelectric and triboelectric methods, only dynamic touch events can be detected. In the former two cases, the leakage currents induced by the imperfect insulating properties of piezoelectric materials result in a decrease in signal, preventing the successful detection of static touch signals. In the latter case, friction is required for charge generation. Hence, static touches cannot be interpreted with these techniques. Hover touches, which are used for gesture sensing in optical and capacitive techniques, cannot be sensed by these technologies. Nevertheless, these approaches can be combined with capacitive sensing to achieve short-distance hover touch detection. For example, in [22], a high-frequency band (100 kHz) was utilized for capacitive sensing, while a low-frequency band (DC to 10 kHz) was employed for force-touch-induced electrical signals, potentially enabling hover touch detection. Due to the temperature isolation between a gloved finger and the surface of the touch panel, glove touch is not supported by pyroelectric and thermoelectric touch panels.

**Table 2.** Comparison of Functional-Material-Based Touch Panels

Working Principle	External Physical Stimuli	Multidimensional?	Positive or Passive?	Multitouch Supported?	Static or Dynamic Touch Supported?	Hover Touch Supported?	Glove Touch Supported?
Piezoelectric	Force	3D	Passive	No	Dynamic	No	Yes
Piezoresistive	Force	3D	Positive	No	Both	No	Yes
Triboelectric	Force	3D	Passive	No	Dynamic	No	Yes
Pyroelectric	Temperature	2D	Passive	Yes	Both	No	No
Thermoelectric	Temperature	2D	Passive	Yes	Both	No	No

**Table 3.** Potential Application Scenarios

Working Principle	Commercial Smartphone	Vehicle Display	Underwater Display	Large-Area Display	Curved or Flexible Display
Piezoelectric	Yes	Yes	Yes	Yes	Yes
Piezoresistive	Yes	Yes	Yes	Yes	Yes
Triboelectric	Yes	Yes	Yes	Yes	Yes
Pyroelectric	Yes	No	No	Yes	Yes
Thermoelectric	Yes	No	No	Yes	Yes

Based on the above analysis and comparison of functional-material-based touch panels, their potential uses in conventional and forthcoming interactive displays are briefly summarized here. For commercial smartphones, tablets and laptops intended for daily use, all of these techniques are suitable. Although these techniques could also be used in large-area displays, optical methods are more widely used in such applications because of their less complex circuitry, ease of installation and lower cost. For vehicle and underwater displays, temperature-related sensing methods are not recommended because of the likelihood that the user will be wearing gloves. With regard to curved and flexible displays, which are now attracting global attention and are expected to enter the market soon, all reviewed techniques enable position detection, although 3D detection suffers in terms of detection accuracy due to the unpredictable boundary conditions (especially for flexible displays); the details will be discussed in Section IV.

## 4. Challenges and Trends

The previous section briefly summarized the use of functional materials in touch interfaces for multidimensional sensing. However, some challenges remain that prevent the successful use of functional materials in commercial human-machine interfaces (HMIs) for multidimensional sensing. This section first explains these challenges and then discusses and predicts potential development trends.

### 4.1 Multiple Superimposed Stimuli

A user-touch-induced electric signal is a combination of multiple physical phenomena. For example, when a user taps the surface of a piezoelectric touch panel, triboelectrification inevitably also occurs. Thus, the detected signal arises from a combination of the piezoelectric and triboelectric effects. However, the discrimination of the piezoelectric signal from the combined signal has not yet been reported in the literature. Another example is the combination of the piezoelectric and pyroelectric effects

that occurs when ferroelectric materials, e.g., PVDF, are used. For example, pyroelectric detectors will generate unwanted output voltages due to environmental effects such as rapid changes in ambient temperature or mechanical vibration. In addition, pyroelectric detectors used in a high-vibration or acoustically noisy environment may produce microphonic noise signals that can be very significant. Although it has been reported that heat transfer is slower than the piezoelectric response<sup>[23]</sup>, the successful separation of these two effects has not yet been presented for interactive display applications. Hence, there is a need to achieve the precise detection of a single physical effect to provide customers with higher detection accuracy and to enable potential applications.

### 4.2 Unstable Responsivity Induced by User Touch Behaviors

The second challenge stems from the manner of human-machine interactions. Touch actions can be performed by users in a variety of ways. For example, finger touches with the same force amplitude can strike the touch panel from different angles, at different speeds, and with diverse contact areas, resulting in unstable force-voltage responsivity in piezoelectric touch panels and thus decreasing the detection accuracy<sup>[43]</sup>. Another example arises with the use of the pyroelectric and thermoelectric techniques, which rely on the temperature difference between a human finger and its touch location. The electrical output suffers from instability due to temperature differences between touch objects. For instance, a bare human finger and a gloved finger have different temperatures; hence, the amplitudes of the corresponding thermal touch-induced electrical signals vary<sup>[23]</sup>.

### 4.3 Lack of Efficient Calibration

A calibration mechanism is vital for most, if not all, sensing systems. However, current studies have focused on achieving high sensing performance (e.g., sensitivity and responsivity) of functional-material-based touch panels but have failed to design calibration functions for maintaining this high performance over long-term use. For example, when the mechanical properties of a touch panel change, e.g., due to being occasionally dropped on the floor, its boundary conditions will be altered; consequently, the force-voltage responsivity of piezoelectric and triboelectric touch panels will change accordingly. Although external commercial force sensors could be used periodically for calibration, this would be inconvenient for customers, and we cannot expect customers to purchase additional equipment to use our products. Even real-time

calibration, also referred to as compensation, may be required. For example, the temperature of an interactive display will typically increase during operation. Hence, calibration/compensation mechanisms must be designed as part of pyroelectric and thermoelectric touch sensing technologies. The lack of such functions will result in only 2-dimensional sensing being achieved in multifunctional touch panels.

## 5. Conclusion

Thanks to the rapid development of mobile and portable electronics, touch interfaces are now almost omnipresent for use in interpreting user commands at end terminals. To boost the efficiency of data exchange between humans and machines and to provide users with advanced/novel experiences, functional-material-based touch panels for multidimensional sensing have been proposed and implemented in recent years. In this work, we have illustrated how simply structured functional-material-based touch interfaces with low costs and low power requirements can detect multidimensional stimuli by means of a review of their working principles and the current state of the art in touch panels assembled from piezoelectric, piezoresistive, triboelectric, pyroelectric, and thermoelectric materials. The work presented here offers readers a picture of the potential development trends of touch interfaces, which are becoming fundamental components in interactive displays, the Internet of Things, and smart cities.

## References

- [1] A. Nathan and S. Gao. Interactive Displays: The Next Omnipresent Technology [Point of View]. Proceedings of the IEEE, 2016, 104(8): 1503-1507.
- [2] G. Walker. A review of technologies for sensing contact location on the surface of a display. Journal of the Society of Information Display, 2012, 20(8): 413-440.
- [3] S. H. Park, H. S. Kim, J. S. Bang and G. H. Cho, and Cho. A 0.26-nJ/node, 400-kHz Tx driving, filtered fully differential readout IC with parasitic RC Time delay reduction technique for 65-in capacitive-type touch screen panel. IEEE Journal of Solid-State Circuits, 2017, 52(2): 528-542.
- [4] A. T. Fried, S. W. Tanamachi, J. T. Abrahamson and R. J. Monson. Qualification of silver nanowire transparent conductive films for touch panel applications. In 2014 IEEE 14th International Conference on Nanotechnology (IEEE-NANO), 2014: 24-26.
- [5] M. D. Ker, P. Y. Chiu, W. T. Shieh and C. C. Wang. ESD Protection design for touch panel control IC against latchup-like failure induced by system-level ESD test. IEEE Transactions on Electron Devices 2017; 64(2): 642-645.
- [6] S. Blayac, A. Schreiner, M. Nouaille, B. Dubois and F. Depoutot. Single port, large area touch and force sensing: Towards low cost sensitive printed surfaces. In 2014 IEEE Ninth International Conference on Intelligent Sensors, Sensor Networks and Information Processing (ISSNIP), 2014: 1-6.
- [7] Z. Ye, M. Wong, M. T. Ng, K. H. Chui, C. K. Kong, L. Lu, and J. K. Luo. High precision active-matrix self-capacitive touch panel based on fluorinated ZnO thin-film transistor. Journal of Display Technology, 2015, 11(1): 22-29.
- [8] C. C. Lee, J. C. Ho, K. J. Chen, M. H. Yeh, Y. Z. Lee and J. Chen. Highly flexible AMOLED integrated with ultrathin on-cell touch panel. In 2016 IEEE Photonics Conference (IPC), 2016: 665-666.
- [9] Y. M. Chiang, Y. L. Lin and W. H. Chien. Automated surface defect inspection system for capacitive touch sensor. In 2015 7th International Conference of Soft Computing and Pattern Recognition (SoCPaR), 2015: 274-277.
- [10] C. L. Lin, T. C. Chu, C. E. Wu, Y. M. Chang, T. C. Lin, J. F. Chen and W. C. Chiu. Tracking Touched Trajectory on Capacitive Touch Panels Using an Adjustable Weighted Prediction Covariance Matrix. IEEE Transactions on Industrial Electronics, 2017, 64(6): 4910-4916.
- [11] S. J. Wu, Y. C. Wu, H. H. Tsai, H. H. Liao, Y. Z. Juang and C. H. Lin. ISFET-based pH sensor composed of a high transconductance CMOS chip and a disposable touch panel film as the sensing layer. In 2015 IEEE SENSORS Conference, 2015: 1-4.
- [12] L. Du, C. Liu, A. Tang, Y. Zhang, Y. Li, K. Cheung and M. C. F. Chang. Airtouch: A novel single layer 3D touch sensing system for human/mobile devices interactions. In 2016 53rd ACM/EDAC/IEEE Design Automation Conference (DAC), 2016, 1-6.
- [13] C. L. Lin, Y. M. Chang, C. C. Hung, C. D. Tu and C. Y. Chuang. Position estimation and smooth tracking with a fuzzy-logic-based adaptive strong tracking Kalman filter for capacitive touch panels. IEEE Transactions on Industrial Electronics, 2015, 62(8): 5097-5108.
- [14] P. Y. L. Lee, C. W. Lu, C. C. Hsieh, T. Y. Chang, J. Y. C. Liu, H. C. Liang and H. N. Wu. Electric hum signal readout circuit for touch screen panel applications. Journal of Display Technology, 2016, 12(11): 1444-1450.
- [15] S. H. Lee, J. S. An, S. K. Hong and O. K. Kwon. In-cell capacitive touch panel structures and their readout circuits. In 2016 IEEE The 23rd International

- Workshop on Active-Matrix Flatpanel Displays and Devices (AMFPD), 2016: 258-261.
- [16] Y. C. Wu, S. J. Wu and C. H. Lin. High performance EGFET-based pH sensor utilizing low-cost industrial-grade touch panel film as the gate structure. *IEEE Sensors Journal*, 2015, 15(11): 6279-6286.
- [17] C. Kim, D. S. Lee, J. H. Kim, H. B. Kim, S. R. Shin, J. H. Jung,... and G. T. Kim. 60.2: Invited Paper: Advanced In-cell Touch Technology for Large Sized Liquid Crystal Displays. In *SID Symposium Digest of Technical Papers*, 2015, 46(1): 895-898.
- [18] H. Akhtar and Q. Kema. An accurate and efficient sampling algorithm for capacitive touch panels. In *Instrumentation and Measurement Technology Conference Proceedings (I2MTC)*. *IEEE International*, 2016: 1-6.
- [19] N. Miura, S. Dosho, S. Takaya, D. Fujimoto, T. Kiriya, H. Tezuka and M. Nagata. 12.4 A 1mm-pitch 80× 80-channel 322Hz-frame-rate touch sensor with two-step dual-mode capacitance scan. In *Solid-State Circuits Conference Digest of Technical Papers (ISS-CC)*, *IEEE International*, 2014: 216-217.
- [20] S. Kim, S. Cho, Y. Pu, S.S. Yoo, M. Lee, K.C. Hwang, Y. Yang and K.Y. Lee. A 39.5-dB SNR, 300-Hz Frame-Rate, 56× 70-Channel Read-Out IC for Electromagnetic Resonance Touch Panels. *IEEE Transactions on Industrial Electronics*, 2018, 65(6): 5001-5011.
- [21] O. Raymudo. Iphone 6S display teardown reveals how 3D touch sensors actually work. *Message Posted to Macworld*, 2015.
- [22] S. Gao, X. Wu, H. Ma, J. Robertson and A. Nathan. Ultrathin multifunctional graphene-PVDF layers for multidimensional touch interactivity for flexible displays. *ACS Applied Materials & Interfaces* 2017, 9(22): 18410-18416.
- [23] T. Vuorinen, M. Zakrzewski, S. Rajala, D. Lupo, J. Vanhala, K. Palovuori and S. Tuukkanen. Printable, transparent and flexible touch panels working in sunlight and moist environments. *Advanced Functional Materials*, 2014, 24(40): 6340-6347.
- [24] S. Gao, V. Arcos and A. Nathan. Piezoelectric vs. Capacitive Based Force Sensing in Capacitive Touch Panels. *IEEE Access*, 2016, 4: 3769-3774.
- [25] T. Jin, J. Ryu, H. Kang, K. No and S.H.K. Park. 46-2: Multi-level-pressure touch sensors with P (VDF-TrFE) deposited on metal oxide thin film transistor. *SID Symposium Digest of Technical Papers*, 2016, 47(1): 621-624.
- [26] C. C. Kim, H. H. Lee, K. H. Oh and J. Y. Sun. Highly stretchable, transparent ionic touch panel. *Science*, 2016, 353(6300): 682.
- [27] G. Sari, M. B. Akgül, B. Kirişken, A. F. Ak and A. A. Akiş. An experimental study of a piezoelectrically actuated touch screen. *Mechanical and Aerospace Engineering (ICMAE)*, 8th International Conference, 2017: 753-758.
- [28] S. Yue and W. A. Moussa. A piezoresistive tactile sensor array for touchscreen panels. *IEEE Sensors Journal*, 2017, 18(4): 1685-1693.
- [29] M. Ruoho, T. Juntunen, T. Alasaarela, M. Pudas and I. Tittonen. Transparent, flexible, and passive thermal touch panel. *Advanced Materials Technologies*, 2016, 1(9).
- [30] D. D. Liana, B. Raguse, J. J. Gooding and E. Chow. An integrated paper - based readout system and piezoresistive pressure sensor for measuring bandage compression. *Advanced Materials Technologies*, 2016, 1(9).
- [31] J. Wu, L. Wang and J. Li. A handwriting input method based on the thermal cue of the fingertip. *Measurement*, 2016, 91: 557-564.
- [32] X. Wang, H. Zhang, L. Dong, X. Han, W. Du, J. Zhai, C. Pan and Z. L. Wang. Self-powered high-resolution and pressure-sensitive triboelectric sensor matrix for real-time tactile mapping. *Advanced materials*, 2016, 28(15): 2896-2903.
- [33] X. Pu, M. Liu, X. Chen, J. Sun, C. Du, Y. Zhang, J. Zhai, W. Hu and Z. L. Wang. Ultrastretchable, transparent triboelectric nanogenerator as electronic skin for biomechanical energy harvesting and tactile sensing. *Science Advances*, 2017, 3(5): e1700015.
- [34] X. Z. Jiang, Y. J. Sun, Z. Fan and T. Y. Zhang. Integrated flexible, waterproof, transparent and self-powered tactile sensing panel. *ACS Nano*, 2016, 10(8): 7696-7704.
- [35] S. P. Mohanty, U. Choppali and E. Kougiannos. Everything you wanted to know about smart cities: The internet of things is the backbone. *IEEE Consumer Electronics Magazine*, 2016, 5(3): 60-70.
- [36] H. Wang, Q. M. Zhang, L. E. Cross and A. O. Sykes. Piezoelectric, dielectric and elastic properties of poly (vinylidene fluoride/trifluoroethylene). *Journal of Applied Physics*, 1993, 74(5): 3394-3398.
- [37] X. Zhao, et al. Active health monitoring of an aircraft wing with embedded piezoelectric sensor/actuator network: I. Defect detection, localization and growth monitoring. *Smart Materials and Structures*, 2007, 16(4): 1208.
- [38] P. F. Liu, X. J. Meng, J. H. Chu, G. Geneste and B. Dkhil. Effect of in-plane misfit strains on dielectric and pyroelectric response of poly (vinylidene fluoride-trifluoroethylene) ferroelectric polymer. *Journal of Applied Physics*, 2009, 105(11): 114105.

- [39] N. W. Emanetoglu, C. Gorla, Y. Liu, S. Liang and Y. Lu. Epitaxial ZnO piezoelectric thin films for saw filters. *Materials Science in Semiconductor Processing*, 1999, 2(3): 247-252.
- [40] C. Jagadish and S. J. Pearton, Eds. *Zinc oxide bulk, thin films and nanostructures: processing, properties, and applications*. Elsevier, 2011.
- [41] T. Karaki, K. Yan, T. Miyamoto and M. Adachi. Lead-free piezoelectric ceramics with large dielectric and piezoelectric constants manufactured from BaTiO<sub>3</sub> nano-powder. *Japanese Journal of Applied Physics*, 2007, 46(2L): L97.
- [42] N. Ma, B. P. Zhang, W. G. Yang and D. Guo. Phase structure and nano-domain in high performance of BaTiO<sub>3</sub> piezoelectric ceramics. *Journal of the European Ceramic Society*, 2012, 32(5): 1059-1066.
- [43] S. B. Jung and S. W. Kim. Improvement of scanning accuracy of PZT piezoelectric actuators by feed-forward model-reference control. *Precision Engineering*, 1994, 16(1): 49-55.
- [44] B. Li, J. H. You and Y. J. Kim. Low frequency acoustic energy harvesting using PZT piezoelectric plates in a straight tube resonator. *Smart Materials and Structures*, 2013, 22(5): 055013.
- [45] L. Ruan, X. Yao, Y. Chang, L. Zhou, G. Qin and X. Zhang. Properties and Applications of the  $\beta$  Phase Poly (vinylidene fluoride). *Polymers*, 2018, 10(3): 228.
- [46] K. Iniewski. *Smart sensors for industrial applications*. CRC Press, 2016.
- [47] V. J. Hodge, S. O. Keefe, M. Weeks and A. Moulds. Wireless sensor networks for condition monitoring in the railway industry: A survey. *IEEE Transactions on Intelligent Transportation Systems*, 2015, 16(3): 1088-1106.
- [48] D. Calestani, M. Villani, M. Culiolo, D. Delmonte, N. Coppedè and A. Zappettini. Smart composites materials: A new idea to add gas-sensing properties to commercial carbon-fibers by functionalization with ZnO nanowires. *Sensors and Actuators B: Chemical*, 2017, 245: 166-170.
- [49] Z. Huang, Q. Zhang, S. Corkovic, R. Dorey and R. W. Whatmore. Comparative measurements of piezoelectric coefficient of PZT films by berlincourt, interferometer, and vibrometer methods. *IEEE Transactions on Ultrasonics, Ferroelectrics, and Frequency Control*, 2006, 53(12).
- [50] F. Xu, F. Chu and S. Trolier-McKinstry. Longitudinal piezoelectric coefficient measurement for bulk ceramics and thin films using pneumatic pressure rig. *Journal of Applied Physics*, 1999, 86(1): 588-594.
- [51] G. Binnig, C. F. Quate and C. Gerber. Atomic force microscope. *Physical Review Letters*, 1986, 56(9): 930.
- [52] S. Rajala, M. Paajanen and J. Leikkala. Measurement of sensitivity distribution map of a ferroelectret polymer film. *IEEE Sensors Journal* 2016, 16(23): 8517-8522.
- [53] A. Nathan, J. C. Lai and S. Gao, Processing signals from a touchscreen panel. U.S. Patent No. 10/061,434. 2018.
- [54] A. Nathan, J. C. Lai and S. Gao. Touchscreen panel signal processing, U.S. Patent Application 15/421,648, 2017.
- [55] S. H. Bae, O. Kahya, B. K. Sharma, J. Kwon, H. J. Cho, B. Ozyilmaz and J. H. Ahn. Graphene-P (VDF-TrFE) multilayer film for flexible applications. *ACS Nano*, 2013, 7(4): 3130-3138.
- [56] S. Gao, S. and W. Wu. Why Piezoelectric Force Sensing is not successful in interactive displays. accepted in *IEEE Consumer Electronics Magazines*, 2018.
- [57] M. Hrovat, D. Belavic, K. Makarovic, J. Cilenšek and B. Malic. Characterisation of thick-film resistors as gauge sensors on different ltcc substrates. *Informacije MIDEM*, 2014, 44(1): 4-11.
- [58] C. Song, D. V. Kerns, J. L. Davidson and W. Kang. Evaluation and design optimization of piezoresistive gauge factor of thick-film resistors. *Southeastcon '91. IEEE Proceedings of*, 1991, 21: 1106-1109.
- [59] S. Stassi, V. Cauda, G. Canavese and C. F. Pirri. Flexible tactile sensing based on piezoresistive composites: a review. *Sensors*, 2014, 14(3): 5296-332.
- [60] R. S. Karmakar, Y. J. Lu, Y. Fu, K. C. Wei, S. H. Chan and M. C. Wu. Cross-talk immunity of pedot:pss pressure sensing arrays with gold nanoparticle incorporation. *Scientific Reports*, 2017, 7(1): 12252.
- [61] P. Rita, G. Loriga, and N. Taccini. A wearable health care system based on knitted integrated sensors. *IEEE Transactions on Information Technology In Biomedicine*, 2005, 9(3): 337-344.
- [62] T. Mochizuki, et al. Fabrication of flexible transparent electrodes using PEDOT:PSS and application to resistive touch screen panels. *Journal of Applied Polymer Science*, 2018, 135(10): 45972.
- [63] S. F. Tseng, W. T. Hsiao, K. C. Huang and D. Chiang. Electrode patterning on PEDOT:PSS thin films by pulsed ultraviolet laser for touch panel screens. *Applied Physics A*, 2013, 112(1): 41-47.
- [64] Z. L. Wang. Triboelectric nanogenerators as new energy technology for self-powered systems and as active mechanical and chemical sensors. *ACS Nano*, 2013, 7(11): 9533-9557.
- [65] L. Dascalescu, C. Dragan, M. Bilici and R. Chere-

- ches. Triboelectric phenomena in suction-type dilute-phase pneumatic transportation systems for granular plastics. *IEEE Transactions on Industry Applications*, 2010, 46(4): 1570-1577.
- [66] J. Shen, Z. Li, J. Yu, B. Ding, and Z. Li, et al. Humidity-resisting triboelectric nanogenerator for high performance biomechanical energy harvesting. *Nano Energy*, 2017, 40: 282-288.
- [67] B. Ypsilanti and B. Sanden. Particle reduction through the control of triboelectric charges. *IEEE/SEMI Advanced Semiconductor Manufacturing Conference and Workshop*, 1994: 92-94.
- [68] Y. Zi, et al. Effective energy storage from a triboelectric nanogenerator. *Nature Communications*, 2016, 7: 10987.
- [69] B. Zhang, et al. Rotating-disk-based hybridized electromagnetic-triboelectric nanogenerator for sustainably powering wireless traffic volume sensors. *ACS Nano* 2016, 10(6): 6241-6247.
- [70] H. Guo, et al. A water-proof triboelectric-electromagnetic hybrid generator for energy harvesting in harsh environments. *Advanced Energy Materials*, 2016, 6(6).
- [71] L. Zhang, et al. Lawn structured triboelectric nanogenerators for scavenging sweeping wind energy on rooftops. *Advanced Materials*, 2016, 28(8): 1650-1656.
- [72] Z. Wen, et al. Harvesting broad frequency band blue energy by a triboelectric-electromagnetic hybrid nanogenerator. *ACS Nano*, 2016, 10(7): 6526.
- [73] G. Zhu, Z. H. Lin, Q. S. Jing, P. Bai, C. F. Pan, Y. Yang, Y. S. Zhou and Z. L. Wang. Toward large-scale energy harvesting by a nanoparticle-enhanced triboelectric nanogenerator. *Nano Letter*, 2013, 13: 847-853.
- [74] C. Wu, et al. Wearable Electricity Generators Fabricated Utilizing Transparent Electronic Textiles Based on Polyester/Ag Nanowires/Graphene Core-Shell Nanocomposites. *ACS Nano*, 2016, 10(7): 6449-6457.
- [75] B. Meng, et al. A transparent single-friction-surface triboelectric generator and self-powered touch sensor. *Energy & Environmental Science*, 2013, 6(11): 3235-3240.
- [76] S. Wang, L. Lin and Z. L. Wang. Triboelectric nanogenerators as self-powered active sensors. *Nano Energy*, 2015, 11: 436-462.
- [77] M. L. Seol. Impact of contact pressure on output voltage of triboelectric nanogenerator based on deformation of interfacial structures. *Nano Energy*, 2015, 17: 63-71.
- [78] G. Zhu, et al. Self-Powered, Ultrasensitive, flexible tactile sensors based on contact electrification. *Nano Letters*, 2018, 14(6): 3208-3213.
- [79] H. Guo, et al. A triboelectric generator based on checker-like interdigital electrodes with a sandwiched PET thin film for harvesting sliding energy in all directions. *advanced energy materials*, 2015, 5(1).
- [80] J. W. Zhong, Q. Z. Zhong, F. R. Fan, Y. Zhang, S. H. Wang, B. Hu, Z. L. Wang and J. Zhou. Finger typing driven triboelectric nanogenerator and its use for instantaneously lighting up LEDs. *Nano Energy*, 2013, 2(4): 491-497.
- [81] A. Davidson, A. Buis, and I. Glesk. Toward novel wearable pyroelectric temperature sensor for medical applications. *IEEE Sensors Journal*, 2017, 17(20): 6682 - 6689.
- [82] M. R. H. Sarker, et al. Characterization of the pyroelectric coefficient of a high-temperature sensor. *Journal of Intelligent Material Systems & Structures*, 2017: 1045389X1772137.
- [83] S. A. Pullano, S. K. Islam, and A. S. Fiorillo. Pyroelectric sensor for temperature monitoring of biological fluids in microchannel devices. *IEEE Sensors Journal*, 2014, 14(8): 2725-2730.
- [84] C. Kittel. *Introduction to solid state physics*, 8th edition. *American Journal of Physics*, 2005, 21(8): 547-548.
- [85] J. G. Webster. *The measurement, instrumentation, and sensors handbook*. CRC Press, 1995.
- [86] A. V. Bune, et al. Piezoelectric and pyroelectric properties of ferroelectric Langmuir-Blodgett polymer films. *Journal of applied physics*, 1999, 85(11): 7869-7873.
- [87] R. W. Whatmore. *Pyroelectric devices and materials, Infrared Detectors and Emitters: Materials and Devices*. *Electronic Materials Series*, 2001, 8. Springer, Boston, MA
- [88] Y. J. Ko, B. K. Yun and J. H. Jung. A 0.7 Pb (Mg 1/3 Nb 2/3) O 3-0.3 PbTiO 3-based pyroelectric generator and temperature sensor. *Journal of the Korean Physical Society*, 2015, 66(4): 713-716.
- [89] J. Zheng and Y. Tu. Based on GSM wireless fire alarm system. *International Journal of Computer Applications*, 2016, 133(9): 38-40.
- [90] Haidong Xu, et al. Ceiling mount intrusion detector with arbitrary direction detection capability. U.S. Patent No. 9,830,789. 28, 2017.
- [91] V. Spagnolo, P. Patimisco, R. Pennetta, A. Sampao, G. Scamarcio, M. S. Vitiello and F. K. Tittel. THz Quartz-enhanced photoacoustic sensor for H 2 S trace gas detection. *Optics Express*, 2015, 23(6): 7574-7582.
- [92] M. Dong, G. Q. Zhong, S. Z. Miao, C. T. Zheng and

- Y. D. Wang. CO and CO<sub>2</sub> dual-gas detection based on mid-infrared wideband absorption spectroscopy. *Optoelectronics Letters*, 2018, 14(2): 119-123.
- [93] G. P. Eppeldauer, V. B. Podobedov, L. M. Hanssen and C. C. Cooksey. Low-NEP pyroelectric detectors for calibration of UV and IR sources and detectors. *International Society for Optics and Photonics*, 2017, 10378: 1037809.
- [94] A. Steiger, W. Bohmeyer and K. Lange. Novel pyroelectric detectors applied for precise THz power measurements. *OSA CLEO: QELS\_Fundamental Science*, 2016.
- [95] R. Müller, B. Gutschwager, J. Hollandt, M. Kehrt, C. Monte, R. Müller and A. Steiger. Characterization of a large-area pyroelectric detector from 300 GHz to 30 THz. *Journal of Infrared, Millimeter, and Terahertz Waves*, 2015, 36(7): 654-661.
- [96] L. Hu, H. Wu, T. Zhu, C. Fu, J. He, P. Ying and X. Zhao. Tuning Multiscale Microstructures to Enhance Thermoelectric Performance of n-Type Bismuth-Telluride-Based Solid Solutions. *Advanced Energy Materials*, 2015, 5(17): 1500411.
- [97] M. Romdhane, C. Gourdon, and G. Casamatta. Development of a thermoelectric sensor for ultrasonic intensity measurement. *Ultrasonics*, 1995, 33(2): 139-146.
- [98] M. Müller, et al. A thermoelectric infrared radiation sensor with monolithically integrated amplifier stage and temperature sensor. *Sensors and Actuators A: Physical*, 1996, 54(1): 601-605.
- [99] J. Eskandari. Thermoelectric cooler and temperature sensor subassembly with improved temperature control. U.S. Patent No. 5,522,225, 1996.
- [100] B. Sothmann, R. Sánchez and A. N. Jordan, A. N. Thermoelectric energy harvesting with quantum dots. *Nanotechnology*, 2014, 26(3): 032001.
- [101] F. J. DiSalvo. Thermoelectric cooling and power generation. *Science*, 1999, 285(5428): 703-706.
- [102] D. Zhao and G. Tan. A review of thermoelectric cooling: materials, modeling and applications. *Applied Thermal Engineering*, 2014, 66(1-2): 15-24.
- [103] G. Min and D. M. Rowe. Cooling performance of integrated thermoelectric microcooler. *Solid-State Electronics*, 1999, 43(5): 923-929.
- [104] Y. K. Ramadass and A. P. Chandrakasan. A battery-less thermoelectric energy harvesting interface circuit with 35 mV startup voltage. *IEEE Journal of Solid-State Circuits*, 2011, 46(1): 333-341.
- [105] S. Priya and D. J. Inman, Eds. *Energy harvesting technologies*. New York: Springer, 2009, 21.
- [106] J. P. Im, S. W. Wang, S. T. Ryu and G. H. Cho. A 40 mV transformer-reuse self-startup boost converter with MPPT control for thermoelectric energy harvesting. *IEEE Journal of Solid-State Circuits*, 2012, 47(12): 3055-3067.
- [107] F.J. Zhang, et al. Flexible and self-powered temperature–pressure dual-parameter sensors using microstructure-frame-supported organic thermoelectric materials. *Nature Communications*, 2015, 6: 8356.